High-Resolution Continuum Source AAS

The Better Way to Do Atomic Absorption Spectrometry

Bernhard Welz, Helmut Becker-Ross,
Stefan Florek, Uwe Heitmann

WILEY-VCH Verlag GmbH & Co. KGaA

High-Resolution Continuum Source AAS

B. Welz, H. Becker-Ross,
S. Florek, U. Heitmann

Further Titles of Interest:

J. A. C. Broekaert
Analytical Atomic Spectrometry with Flames and Plasmas
2nd Edition
2005, ISBN 3-527-31282-X

E. Merian, M. Anke, M. Ihnat, M. Stoeppler
Elements and their Compounds in the Environment
Occurrence, Analysis and Biological Relevance
3 Volumes, 2nd Edition
2004, ISBN 3-527-30459-2

J. Nölte
ICP Emission Spectrometry
A Practical Guide
2003, ISBN 3-527-30672-2

B. Welz, M. Sperling
Atomic Absorption Spectrometry
3rd Edition
1999, ISBN 3-527-28571-7

High-Resolution Continuum Source AAS

The Better Way to Do Atomic Absorption Spectrometry

Bernhard Welz, Helmut Becker-Ross,
Stefan Florek, Uwe Heitmann

WILEY-VCH Verlag GmbH & Co. KGaA

Authors

Prof. Dr. Bernhard Welz
Departamento de Química
Universidade Federal de Santa Catarina
88040-900 Florianópolis – SC
Brazil

Dr. Helmut Becker-Ross
ISAS – Institute for Analytical Sciences,
Department Berlin
ISAS – Institute for Analytical Sciences,
Department Berlin
Albert-Einstein-Strasse 9
12489 Berlin
Germany

Dr. Stefan Florek
ISAS – Institute for Analytical Sciences,
Department Berlin
Albert-Einstein-Strasse 9
12489 Berlin
Germany

Dr. Uwe Heitmann
ISAS – Institute for Analytical Sciences,
Department Berlin
Albert-Einstein-Strasse 9
12489 Berlin
Germany

Library of Congress Card No.: applied for
British Library Cataloging-in-Publication Data:
A catalogue record for this book is available from the British Library

Bibliographic information published by Die Deutsche Bibliothek
Die Deutsche Bibliothek lists this publication in the Deutsche Nationalbibliografie; detailed bibliographic data is available in the Internet at <http://dnb.ddb.de>.

Printed in the Federal Republic of Germany
Printed on acid-free paper

Printing Druckhaus Darmstadt GmbH, Darmstadt
Bookbinding Litges & Dopf Buchbinderei GmbH, Heppenheim

ISBN-13: 978- 3-527-30736-4
ISBN-10: 3-527-30736-2

Preface

Conventional line source atomic absorption spectrometry (LS AAS) can nowadays be considered an established technique in the positive sense of the term, i.e. it is widely used, and no dramatic improvements are expected in the foreseeable future. The state-of-the-art of conventional LS AAS is fully described in the book of Welz and Sperling [150], and its content may well be valid for another decade or two. The only progress will be in the development of new applications, but this field is today fully covered by a variety of data banks, which are easily accessible through the Internet, so that this increase in literature on applications does not justify a new edition of this book.

The only real progress in the field of AAS, in the opinion of the authors, is in the direction of high-resolution continuum source AAS (HR-CS AAS), which will undoubtedly be the future of this technique. For this reason we thought it would be much more useful to write a new book about HR-CS AAS, which might be considered a 'Volume 2' or a 'Supplement' of the above basic book on AAS. This means we expect the reader of this book to be aware of the basic concepts of AAS, which is fully covered in Reference [150], and so we have deliberately avoided repeating things in this book that have been described in the former one. For example, neither the different atomizers used in AAS, i.e. flame, graphite furnace or quartz tube atomizers, nor the atomization mechanisms or the non-spectral interferences occurring in these atomizers are discussed in this book, as they are obviously identical. In essence, only the new aspects and developments that are particular to HR-CS AAS are discussed in detail, whereas common things are repeated only where absolutely necessary.

The content of this book, regarding practical application, has essentially been produced over a time period of less than two years using prototype instruments, which are similar, but not identical, to the commercially available instrument. There have been an impressive number of people, master, doctoral and post-doctoral students, working with these prototypes, but obviously we can only give examples for the application of this new technique, not a full coverage of all the possibilities. We expect that you, the readers of this book, who hopefully will be using this exciting new technique, will be contributing

to the exploration of the potential of HR-CS AAS so that the second edition of this book will contain a much more complete coverage of yet undiscovered application possibilities of this new technique.

This book is an integral part of the professorial dissertation of Uwe Heitmann. He has written several chapters and was responsible for the preparation of the figures as well as for the total arrangement and layout of this book up to the delivery of a ready-for-press manuscript. Uwe Heitmann has been concerned with the HR-CS AAS project since 1994. He was involved in most of the measurements, their evaluation and interpretation. Moreover, he carried out the setup of the prototype instruments and wrote the in-house software for data acquisition, signal processing and background correction.

Florianópolis, Berlin, December 2004

Bernhard Welz
Helmut Becker-Ross
Stefan Florek
Uwe Heitmann

Contents

1. Historical Development of Continuum Source AAS **1**

2. Theoretical Concepts **5**

2.1 Spectral Line Profiles 5
2.1.1 Natural Line Width 5
2.1.2 Doppler Broadening 6
2.1.3 Collision Broadening 7
2.1.4 Voigt Profiles 8
2.1.5 Instrument Profile 11
2.2 Atomic Absorption with a Continuum Source 17
2.2.1 General Principle of Absorption 17
2.2.2 Instrument Effects 18
2.3 Structure of Molecular Spectra 24
2.3.1 Electronic Transitions 24
2.3.2 Vibrational Spectra 26
2.3.3 Rotational Spectra 28
2.3.4 Dissociation Continua 30

3. Instrumentation for HR-CS AAS **31**

3.1 Radiation Source 31
3.2 Research Spectrometers with Active Wavelength Stabilization 34
3.2.1 Echelle Grating 35
3.2.2 Sequential Spectrometer 37
3.2.3 Simultaneous Spectrometer 46
3.3 Detector 50
3.4 The contrAA 300 from Analytik Jena AG 53

4. Special Features of HR-CS AAS 57

4.1 The Modulation Principle 57
4.2 Simultaneous Double-beam Concept 58
4.3 Selection of Analytical Lines 59
4.4 Sensitivity and Working Range 62
4.5 Signal-to-Noise Ratio, Precision and Limit of Detection 68
4.6 Multi-element Atomic Absorption Spectrometry 72
4.7 Absolute Analysis 74

5. Measurement Principle in HR-CS AAS 77

5.1 General Considerations 77
5.2 Background Measurement and Correction 79
5.2.1 Continuous Background 79
5.2.2 Fine-structured Background 85
5.2.3 Direct Line Overlap 89

6. The Individual Elements 91

6.1 Aluminum (Al) 94
6.2 Antimony (Sb) 97
6.3 Arsenic (As) 98
6.4 Barium (Ba) 98
6.5 Beryllium (Be) 99
6.6 Bismuth (Bi) 99
6.7 Boron (B) 101
6.8 Cadmium (Cd) 102
6.9 Calcium (Ca) 103
6.10 Cesium (Cs) 103
6.11 Chromium (Cr) 104
6.12 Cobalt (Co) 106
6.13 Copper (Cu) 108
6.14 Europium (Eu) 109
6.15 Gallium (Ga) 109
6.16 Germanium (Ge) 110
6.17 Gold (Au) 111
6.18 Indium (In) 111
6.19 Iridium (Ir) 112
6.20 Iron (Fe) 112
6.21 Lanthanum (La) 114

6.22 Lead (Pb) . . . 115
6.23 Lithium (Li) . . . 116
6.24 Magnesium (Mg) . . . 117
6.25 Manganese (Mn) . . . 117
6.26 Mercury (Hg) . . . 120
6.27 Molybdenum (Mo) . . . 121
6.28 Nickel (Ni) . . . 122
6.29 Palladium (Pd) . . . 124
6.30 Phosphorus (P) . . . 125
6.31 Platinum (Pt) . . . 127
6.32 Potassium (K) . . . 128
6.33 Rhodium (Rh) . . . 128
6.34 Rubidium (Rb) . . . 128
6.35 Ruthenium (Ru) . . . 129
6.36 Selenium (Se) . . . 129
6.37 Silicon (Si) . . . 130
6.38 Silver (Ag) . . . 133
6.39 Sodium (Na) . . . 133
6.40 Strontium (Sr) . . . 135
6.41 Sulfur (S) . . . 135
6.42 Tellurium (Te) . . . 137
6.43 Thallium (Tl) . . . 138
6.44 Tin (Sn) . . . 139
6.45 Titanium (Ti) . . . 141
6.46 Tungsten (W) . . . 141
6.47 Vanadium (V) . . . 142
6.48 Zinc (Zn) . . . 144

7. Electron Excitation Spectra of Diatomic Molecules 147

7.1 General Considerations . . . 147
7.2 Individual Overview Spectra . . . 153
7.2.1 AgH . . . 155
7.2.2 AlCl . . . 158
7.2.3 AlF . . . 160
7.2.4 AlH . . . 162
7.2.5 AsO . . . 164
7.2.6 CN . . . 166
7.2.7 CS . . . 169

7.2.8 CuH . . . 173
7.2.9 GaCl . . . 176
7.2.10 LaO . . . 178
7.2.11 NH . . . 179
7.2.12 NO . . . 180
7.2.13 OH . . . 185
7.2.14 PO . . . 190
7.2.15 SH . . . 197
7.2.16 SiO . . . 198
7.2.17 SnO . . . 205

8. Specific Applications 211
8.1 Flame Measurements . . . 211
8.1.1 Molecular Background in Flame AAS . . . 211
8.1.2 Drinking Water Analysis . . . 213
8.1.3 Sodium and Potassium in Animal Food and Pharmaceutical Products . . . 215
8.1.4 Determination of Zinc in Iron and Steel . . . 215
8.1.5 Determination of Trace Elements in High-purity Copper . . . 216
8.1.6 Determination of Phosphorus via PO Molecular Absorption Lines 219
8.1.7 Determination of Sulfur in Cast Iron . . . 223
8.2 Graphite Furnace Measurements . . . 224
8.2.1 Method Development for Graphite Furnace Analysis . . . 224
8.2.2 Direct solid sample analysis . . . 235
8.2.3 Urine Analysis . . . 237
8.2.4 Analysis of Biological Materials . . . 245
8.2.5 Analysis of Seawater . . . 251
8.2.6 Analysis of Soils and Sediments . . . 253
8.2.7 Analysis of Coal and Coal Fly Ash . . . 256
8.2.8 Analysis of Crude Oil . . . 260
8.2.9 Determination of Arsenic in Aluminum . . . 265

9. Outlook 269

References 273

Acknowledgment 283

Index 285

List of Physical Constants, Symbols and Abbreviations

Physical constant	Meaning
c	Speed of light ($2.998 \cdot 10^8$ m/s)
h	Planck's constant ($6.626 \cdot 10^{-34}$ J s)
k_B	Boltzmann's constant ($1.381 \cdot 10^{-23}$ J/K)

Symbol	Meaning [unit, as not indicated otherwise]
A	Absorbance
A_int	Time-integrated absorbance [s]
c_0	Characteristic concentration [μg/L]
λ	Wavelength [nm]
m_0	Characteristic mass [pg]
ν	Frequency [1/s]
τ	Lifetime [ns]

Abbreviation	Meaning
AAS	Atomic absorption spectrometry
AC	Alternating current
ARES	Array echelle spectrograph
BC	Background correction
BCP	Background correction pixel
BOC	Background offset correction
CCD	Charge-coupled device
CRM	Certified reference material
CP	Center pixel
CS	Continuum source
DC	Direct current
DEMON	Double echelle monochromator
DSI	Dispersive slit illumination
ETV	Electro-thermal vaporization
F	Flame
FSR	Free spectral range
FWHM	Full width at half maximum
GF	Graphite furnace
HCL	Hollow cathode lamp
HFS	Hyper-fine structure
HR	High-resolution
ICP	Inductively-coupled plasma
LOD	Limit of detection
LS	Line source
MS	Mass spectrometry
OES	Optical emission spectrometry
PDA	Photodiode array
Pixel	Picture element
PMT	Photo-multiplier tube
SNR	Signal-to-noise ratio
UV	Ultra-violet
VUV	Vacuum-UV
WIA	wavelength integrated absorbance
WSA	wavelength selected absorbance

1. Historical Development of Continuum Source Atomic Absorption Spectrometry

When Bunsen and Kirchhoff [79–81] were carrying out their systematic investigation of the 'line reversal' in alkali and alkaline earth elements, i.e. the correlation between emission and absorption of radiation by atoms, in the early 1860s, they used a continuum source, i.e. 'white light', for their absorption measurements. The few researchers that used atomic absorption for their investigations in the second half of the 19th century, such as Lockyer [92], used similar equipment, as shown in Figure 1.1, for obvious reasons: Firstly, continuum light sources were the only reliable sources available at that time, and secondly, they served perfectly the purpose of detecting and measuring the 'black lines', i.e. the interruptions in the otherwise continuous spectrum, caused by atomic absorption.

In the first half of the 20th century, when atomic spectra were increasingly used not only for the qualitative identification, but also for the quantitative determination of elements, it was at least in part because of this continuum source that spectroscopists gave preference to atomic emission over atomic absorption. It is obviously much easier to detect a small radiation in front of a non-emitting, 'black' background, than a small reduction over a narrow spectral range of a strong emission. Or, if a photographic plate is used as the detector, as was common practice at that time, it is much easier to quantify a small increase in the opacity ('blackening') of the photographic layer than a small decrease in the opacity of an otherwise black plate. Hence, the radiation source was obviously the reason why atomic absorption was essentially excluded from analytical atomic spectroscopy for more than half a century.

It was only in 1952 when Alan Walsh, after having worked on the spectrochemical analysis of metals for seven years, and in molecular spectroscopy for another six years, began to wonder why molecular spectra were usually obtained in absorption and atomic

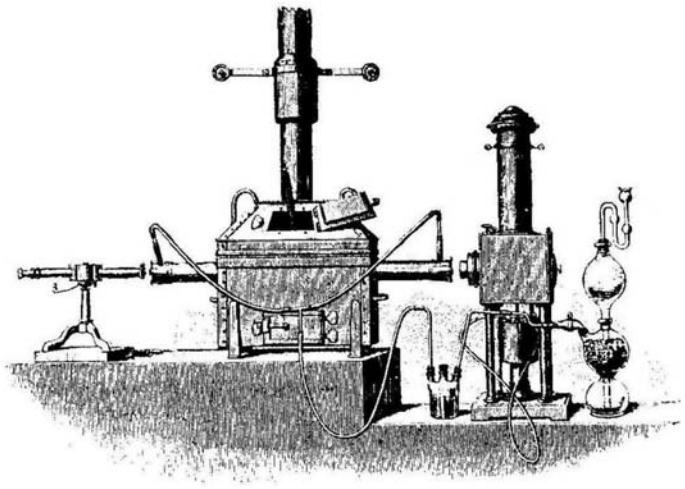

Figure 1.1: Apparatus used by Lockyer [92] for atomic absorption measurements: light source on the right; atomizer in the middle (iron tube mounted in a coal-fired furnace, while hydrogen was generated in a Kipp's apparatus to provide a reducing atmosphere); spectroscope on the left

spectra in emission. The conclusion of his musing was that there was no good reason for neglecting atomic absorption spectra [147]. Obviously, Walsh also had to consider the question of the proper radiation source for recording atomic absorption spectra, and he came to the conclusion that a resolution of approximately 2 pm would be required if a continuum source was used. This was far beyond the capabilities of the best spectrometer available in his laboratory at that time, and he concluded that 'One of the main difficulties is due to the fact that the relations between absorption and concentration depend on the resolution of the spectrograph ...' [147]. This realization led him to conclude that the measurement of atomic absorption requires line radiation sources with the sharpest possible emission lines. The task of the monochromator is then merely to separate the line used for the measurement from all the other lines emitted by the source. The high-resolution demand for atomic absorption measurements is thus provided by the line source.

Anyway, Walsh was quite fortunate because, although the hollow cathode glow had already been discovered back in 1916 by Paschen [114], and had since been used as a fine-line source for spectroscopic investigations, it was only in 1955 that the first sealed-off hollow cathode lamp was constructed [18]. Without this development and the significant

amount of research that Walsh and colleagues put into the improvement of the hollow cathode lamp design, atomic absorption spectrometry (AAS) would probably not have been accepted as a routine technique to the same extent, as it has actually been. The use of modulated line radiation sources and a synchronously tuned detection system, as proposed by Walsh [146], made the AAS technique highly specific and selective, but it obviously also made it a one-element-at-a-time technique, one of the most serious limitations of conventional AAS.

However, although commercial atomic absorption spectrometers have been built exclusively according to the principle proposed by Walsh for more than four decades, research on the use of continuum radiation sources for AAS has continued throughout this period. The early publications in this field [26,30,31,38,41,43,72,103] mainly took advantage of the instability and/or low energy output of hollow cathode lamps for a number of elements, or their unavailability for other elements, particularly the rare-earth elements [31], and demonstrated in this way the superiority of the continuum source approach. Some authors, however, even questioned the validity of Walsh's approach, although the detection limits reported for those elements for which good line sources were available, were at least one order of magnitude inferior with a continuum source.

In the following years, several groups investigated wavelength modulation, using AC scanning [138], oscillating interferometers [109,145] or a combination of optical scanning and mechanical chopping [29] in order to improve the signal-to-noise ratio (SNR) and the sensitivity of continuum source AAS (CS AAS). In the latter work, Elsner and Winefordner reported analytical curves that were linear over at least three orders of magnitude, and detection limits that were close to the theoretical values [29].

A kind of turning point in this early phase of CS AAS was the work of Keliher and Wohlers [78] who for the first time used a high-resolution echelle grating spectrometer for CS AAS. The major limitation at that time was the 150 W xenon lamp used as the continuum source, which had only a relatively low energy at wavelengths below 320 nm, where most of the elements have their most sensitive lines. This work was then continued over the next 25 years by the groups of O'Haver and Harnly [42, 44–54, 90, 93, 104, 106, 107, 110, 136, 137, 157, 161], who continuously improved the system, introducing wavelength modulation [104, 161], a pulsed continuum source and a linear photodiode array detector [48, 49, 106, 107]. They also described the first, and up until now only, functional simultaneous multi-element atomic absorption spectrometer with a continuum source (SIMAAC) [44, 47, 104], and showed the applicability of this system for a variety of practical analytical problems using flame [45, 90] and graphite furnace [46, 93] atomization. The only other 'simultaneous' CS AAS instruments described in the literature [32, 74] used photodiode array detectors that covered a spectral range of 2.5 nm [74] and 10 nm [32], respectively, and only elements that had absorption lines falling within

this narrow spectral window could be detected simultaneously. This approach, obviously, cannot be considered a true simultaneous multi-element system.

In a review article published in 1989, Hieftje [64] provocatively predicted: 'If current trends continue, I would not be surprised to see the removal of commercial AAS instruments from the marketplace by the year 2000.' However, in the same article Hieftje also wrote: 'Clearly, for AAS to remain viable in the face of strong competition from alternative techniques will require novel instrumentation or approaches. Among the novel concepts that have been introduced are those involving continuum sources and high-resolution spectral-sorting devices ... and entirely new detection approaches.' In hindsight, this comment could be considered kind of visionary, as only one decade later, the progress made in CS AAS caused Harnly to forecast in another review article [54] that '... the future appears bright for CS AAS. Whereas, previously, CS AAS was striving for parity with LS AAS, it is now reasonable to state that it is CS AAS which is setting the standard.'

The final breakthrough in CS AAS, however, was not made by Harnly, but by the group of Becker-Ross in Berlin, who had started to work on the development of echelle spectrometers in 1980. Based on their own experience they soon discovered the weak points of the instruments used at that time [110], i.e. the low intensity of conventional xenon arc lamps in the far-UV, and the drawbacks of wavelength modulation with an oscillating quartz plate. Inspired by these ideas they started their own research in this field in 1990 [4–8, 35–37, 58, 60, 126], but with a different approach. Harnly and all the other groups essentially started from commercially available equipment and components, which they assembled and modified according to their needs. Becker-Ross and his colleagues, in contrast, first determined the requirements for CS AAS [5], and then they specified and designed the instrument according to these requirements, starting with the continuum radiation source [4, 126] followed by the spectrometer [6, 35, 36, 58] and then the detector [6, 36, 58]. All details of this concept will be discussed in detail in Chapter 3.

2. Theoretical Concepts

2.1 Spectral Line Profiles

Observed spectral line profiles are governed by a multiplicity of mechanisms, all of which cause spectral line broadening. Three mechanisms are of physical origin and act directly on atoms or molecules when generating or absorbing a photon: natural line broadening, Doppler broadening and collisional or Lorentz broadening. Another effect is of instrumental origin: broadening caused by the characteristics of the spectrometer. In this section the various broadening mechanisms and their interactions are described. The discussion will dispense with all effects of fine structure and hyperfine structure line splitting, because of their element- and line-specific character, which makes a generalized examination impossible. Moreover, except for some prominent outliers, these splitting effects are negligible in comparison to the other broadening effects.

2.1.1 Natural Line Width

Any atom being in an excited state, for instance after absorption of a photon, will undergo a relaxation process to a lower state within a finite time, even if there is no interaction with other atoms or molecules. Typical lifetimes τ for undisturbed excited states are of the order of 10^{-9} to 10^{-8} s. After this the atom re-emits the photon and relaxes to the lower state, which is the ground state in the case of resonance transitions. According to Heisenberg's uncertainty principle $\Delta E\ \Delta t = \hbar$, the finite lifetime τ causes an uncertainty of:

$$\Delta E = \frac{\hbar}{\Delta t} = \frac{h}{2\pi\tau} \tag{2.1}$$

in the energy E of the excited state. Since the transition is associated with a photon energy of $h\nu_0 = E$, the frequency of the photon is also uncertain:

$$\Delta\nu = \frac{\Delta E}{h} = \frac{1}{2\pi\tau}\,. \tag{2.2}$$

If the lower state is not the ground state, it will also show an energy uncertainty corresponding to its own lifetime. In this case $\Delta\nu$ is given by the sum of both contributions.

This uncertainty in frequency, which is inversely proportional to the lifetime, generates a line profile of Lorentz shape, centered at ν_0, with a width $\Delta\nu_\mathrm{N}$. Using the relation $\Delta\lambda_\mathrm{N} = (\lambda^2/c)\,\Delta\nu_\mathrm{N}$ the so-called natural line width $\Delta\lambda_\mathrm{N}$ is obtained and the corresponding wavelength-dependant intensity distribution $I_\mathrm{N}(\lambda)$ of the area-normalized profile is given by:

$$I_\mathrm{N}(\lambda) = \frac{1}{2\pi}\frac{\Delta\lambda_\mathrm{N}}{(\lambda-\lambda_0)^2 + \left(\frac{\Delta\lambda_\mathrm{N}}{2}\right)^2}\,, \tag{2.3}$$

with $\lambda_0 = c/\nu_0$ and a full width at half maximum (FWHM) of:

$$\Delta\lambda_\mathrm{N} = \frac{\lambda^2}{c}\,\frac{1}{2\pi\tau}\,. \tag{2.4}$$

The lifetime of an electron in the excited state in the case of the resonance lines used in AAS is in the range of a few nanoseconds, resulting in $\Delta\lambda_\mathrm{N}$ of about 0.01 pm. This is a small effect compared to the other broadening mechanisms occurring in AAS, and is therefore neglected in the context of this section.

2.1.2 Doppler Broadening

Atomic emission and absorption are always accompanied by a motion of the free atoms during each of the processes. In the case of an emission, the component of the motion in the direction of the radiation causes a frequency shift of the emitted radiation. As statistically the same number of atoms are moving in the direction of observation and in the opposite direction, the frequency shift is acting in both directions, causing a symmetric broadening of the line. In the case of an absorption process, the atoms experience a broadened frequency of the incoming radiation, and the movement of the absorbing atoms causes a further broadening of the line. Both broadening effects are due to the well-known Doppler effect. The frequency shifting effect noticed by an observer is a superposition of all contributions in the direction of the observer's view. If the atoms under consideration are in a thermodynamic equilibrium, the velocity distribution is of Maxwell type and the intensity distribution $I_\mathrm{D}(\lambda)$ seen by the observer may be expressed by a Gaussian profile:

$$I_\mathrm{D}(\lambda) = I(\lambda_0)\exp\left[-\left(\frac{\lambda-\lambda_0}{\frac{1}{\sqrt{4\ln 2}}\,\Delta\lambda_\mathrm{D}}\right)^2\right]\,. \tag{2.5}$$

$\Delta\lambda_\mathrm{D}$, the so-called Doppler line width, is the FWHM which is given by:

$$\Delta\lambda_\mathrm{D} = 2\sqrt{2\ln 2}\,\lambda_0\sqrt{\frac{k_\mathrm{B}T}{c^2 m}}\,. \tag{2.6}$$

If the mass m of the atom is expressed by the molar mass M given in g/mol, the width can be written as:

$$\Delta\lambda_D = 7.16 \cdot 10^{-7}\, \lambda_0 \sqrt{\frac{T}{M}}\,. \tag{2.7}$$

Figure 2.1 shows the wavelength dependence of $\Delta\lambda_D$ for different atom masses. All values are based on a temperature of 2600 K, which is representative for an air / acetylene flame. In the most relevant region, i.e. wavelengths between 190 nm and 350 nm and masses between 14 g/mol and 200 g/mol, the variation of $\Delta\lambda_D$ is in the range 0.5 pm to 3.5 pm.

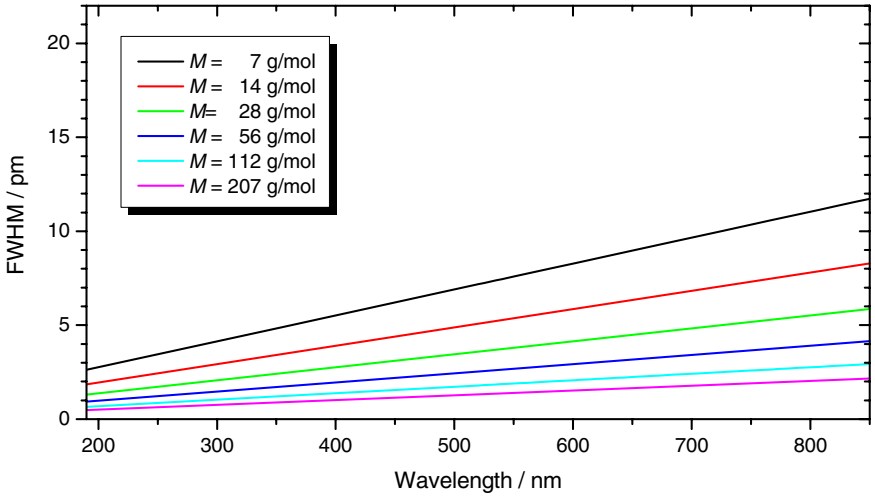

Figure 2.1: Calculated FWHM values for Doppler broadening at 2600 K and different atom masses

2.1.3 Collision Broadening

If the absorbing atoms collide with other atoms or molecules, a further broadening influence on the spectral lines is observed. A thorough discussion of the very complex collisional effects has been published by Allard and Kielkopf [1]. All of these broadening mechanisms produce a Lorentz distribution as line profile corresponding to Equation 2.3. According to Larkins [85] the collisional broadening width $\Delta\nu_C$ expressed in Hz is given by:

$$\Delta\nu_C = \frac{1}{\pi}\, N\, \sigma_C\, \overline{\nu}\,. \tag{2.8}$$

Here, N is the perturbing atom or molecule density, σ_C is the collisional cross-section in m^2, and $\overline{\nu}$ is the mean relative velocity between the colliding partners. For thermal equilibrium $\overline{\nu}$ is given by:

$$\overline{\nu} = \sqrt{\frac{8k_B T}{\pi}\left(\frac{1}{m_A} + \frac{1}{m_B}\right)}\,. \tag{2.9}$$

m_A and m_B are the masses of the absorbing (A) and disturbing (B) atom, respectively. For normal pressure, Equation 2.8 then transforms to:

$$\Delta\nu_C = 1.4 \cdot 10^{16}\,\sigma_C \sqrt{\frac{1}{T}\left(\frac{1}{m_A} + \frac{1}{m_B}\right)}\,. \tag{2.10}$$

Expressed in wavelength and by using molar masses M_A, M_B (g/mol), Equation 2.10 gives the FWHM for collisional broadening, the so-called collisional line width $\Delta\lambda_C$:

$$\Delta\lambda_C = 1.13 \cdot 10^{21}\,\lambda_0^2\,\sigma_C \sqrt{\frac{1}{T}\left(\frac{1}{M_A} + \frac{1}{M_B}\right)}\,. \tag{2.11}$$

Larkins determined collisional cross-sections for some elements in an air / acetylene flame and found a typical value of $\sigma_C \approx 2 \cdot 10^{-18}\,m^2$. Figure 2.2 shows the wavelength dependence of $\Delta\lambda_C$ for this cross-section, a temperature of 2600 K, and different atom masses. As perturbing particle N_2 with $M_B = 28$ has been assumed. In the most relevant region, i.e. wavelengths between 190 nm and 350 nm and masses between 14 g/mol and 200 g/mol, the variation of $\Delta\lambda_C$ spans from 0.5 pm to 2 pm, which is comparable to the range of the Doppler broadening under the same conditions (refer to Figure 2.1).

As well as broadening, a shift of the spectral line appears, which can be towards shorter wavelengths (blue shift) or to longer wavelengths (red shift), depending on the collision partner. For the prominent case of an adiabatic impact, Corney [19] predicted the relationship between shift and broadening to be 0.36.

2.1.4 Voigt Profiles

The observable profile of a spectral line is, in general, neither a pure Lorentz nor a pure Gauss distribution but a combination of both, known as a Voigt profile. If it is assumed that Doppler and collision broadening are independent processes, the Voigt profile is the result of the convolution of the Lorentz distribution with $\Delta\lambda_C$ and the Gauss distribution with $\Delta\lambda_D$. Since the Voigt profile cannot be obtained analytically, numerical convolution procedures have to be applied. A parameter often used for profile characterization is the

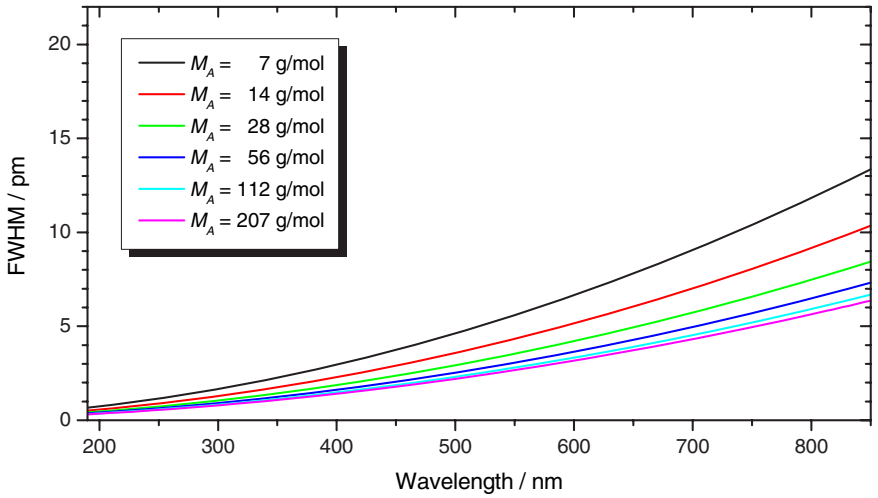

Figure 2.2: Calculated FWHM values for collisional broadening at 2600 K and normal pressure in an air / acetylene flame (perturbing particle: N_2, $M_B = 28$), curve parameter is the atom mass M_A

so-called damping constant α, which is defined as:

$$\alpha = \sqrt{\ln 2}\,\frac{\Delta\lambda_C}{\Delta\lambda_D}\,. \tag{2.12}$$

The FWHM of the Voigt profile, the so-called Voigt line width $\Delta\lambda_V$, cannot be obtained by simple addition of the Doppler and Lorentz widths, but can be approximated by an empirical formula:

$$\Delta\lambda_V \approx \frac{\Delta\lambda_C}{2} + \sqrt{\left(\frac{\Delta\lambda_C}{2}\right)^2 + \Delta\lambda_D^2}\,. \tag{2.13}$$

Figure 2.3 shows Gauss and Lorentz profiles of equal area and FWHM as well as the resulting Voigt distribution. While the Lorentz portion dominates at the line wings, the Gauss portion determines the shape in the line core.

An example of line widths in a conventional air / acetylene flame corresponding to the data in Figures 2.1 and 2.2 is shown in Figure 2.4. The widths of the Voigt profiles are calculated according to Equation 2.13. In the most relevant region, i.e. wavelengths between 190 nm and 350 nm and masses between 14 g/mol and 200 g/mol, the variation of $\Delta\lambda_V$ spans from 0.8 pm to 4.5 pm, but for longer wavelengths and the lighter elements widths of more than 10 pm could be expected.

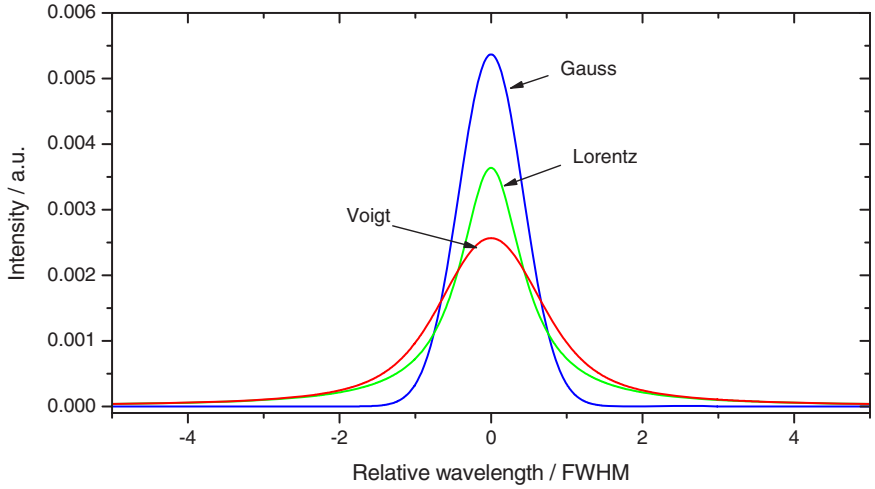

Figure 2.3: Comparison of Gauss (blue line) and Lorentz (green line) curves of equal area and same FWHM, and a Voigt (red line) profile produced by convoluting the other two curves

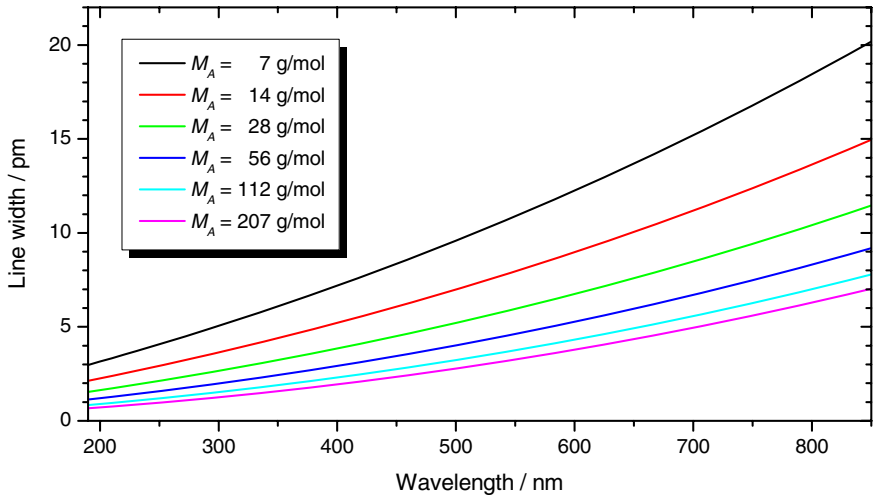

Figure 2.4: Calculated FWHM values for Voigt profiles resulting from Doppler and collisional broadening at 2600 K and normal pressure in an air / acetylene flame (perturbing particle: N_2, $M_B = 28$), curve parameter is the atom mass M_A

2.1.5 Instrument Profile

Although Voigt profiles generally describe the true line shape, every measurement of an intensity distribution by a spectrometer results in an additional influence of the instrument transmittance profile upon this shape. The geometric shape of the instrument profile is determined by the diffraction of the radiation waves, the entrance slit geometry, and the optical aberrations occurring when a monochromatic image of the entrance slit is focused onto the focal plane of the instrument. It can be described as the product of the convolution of a sinc^2 profile with a rectangular shape and a normally non-symmetric aberration distribution. The sinc^2 profile is characterized by the observed wavelength λ_0 and the relative aperture $k_{\mathrm{en}} = f_{\mathrm{en}}/D_{\mathrm{eff}}$ (f_{en}: collimator focal length, D_{eff}: effective collimator diameter) of the instrument. The separation of the first sinc^2 minima from the central maximum is approximately $1.22\ \lambda_0/k_{\mathrm{en}}$. Correspondingly, Δg_{sinc}, the FWHM of the geometric sinc^2 shape can be described as follows:

$$\Delta g_{\mathrm{sinc}} = 1.1\ \frac{\lambda_0}{k_{\mathrm{en}}}\ . \tag{2.14}$$

For real entrance slit widths and negligible aberrations the geometric profile results from the convolution of the sinc^2 with a rectangle. The width of the latter, the entrance slit width s_{en}, can be chosen as $s_{\mathrm{opt}} = 1.22\ \lambda_0/k_{\mathrm{en}}$ to get the optimal geometric instrument profile with a FWHM of:

$$\Delta g^{\mathrm{opt}}_{\mathrm{instr}} = 1.37\ \frac{\lambda_0}{k_{\mathrm{en}}}\ . \tag{2.15}$$

For conversion of geometrical profiles to spectral profiles the geometrical width has to be multiplied by the reciprocal linear dispersion $\delta\lambda/\delta x$ of the instrument giving the width $\Delta\lambda^{\mathrm{opt}}_{\mathrm{instr}}$ of the optimal instrument profile:

$$\Delta\lambda^{\mathrm{opt}}_{\mathrm{instr}} = 1.37\ \frac{\lambda_0}{k_{\mathrm{en}}}\ \frac{\delta\lambda}{\delta x}\ . \tag{2.16}$$

Curve B in Figure 2.5 shows the corresponding profile, which can be described in good approximation by a Gauss function. Larger slit widths lead to more or less rectangular profiles, as can be observed in case a multi-pixel photo detector is used in the focal plane and the pixel width is significantly smaller than the entrance slit width. An illustration of these conditions is also given in Figure 2.5.

As an example of the validity of the above-mentioned description of the different broadening mechanisms, Figures 2.6, 2.7, and 2.8 show a comparison of calculated and measured line profiles as can be expected in a normal air / acetylene flame. In a first step the Cu doublet at 324.754 nm was measured with the high-resolution echelle spectrometer

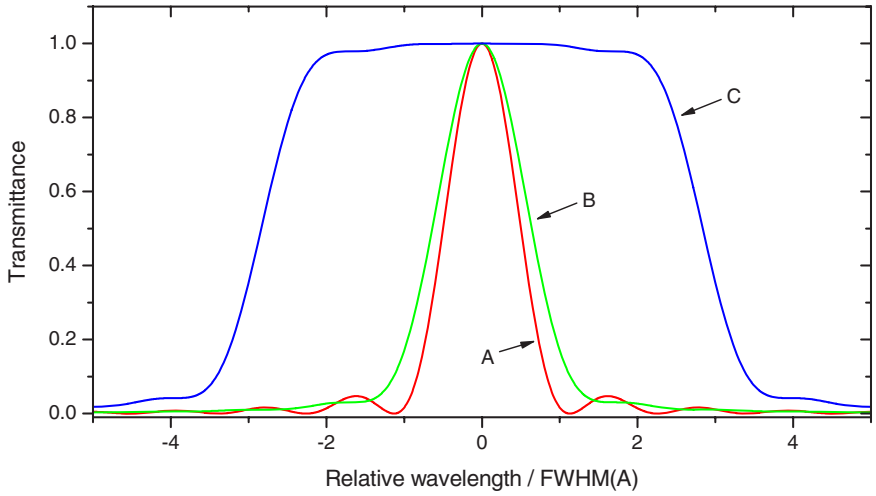

Figure 2.5: Calculated instrument profiles for three different entrance slit widths s_{en}; A: $s_{en} = 0$ (pure sinc^2 profile); B: profile A convoluted by a rectangular profile with $s_{en} = s_{opt}$; C: profile A convoluted by a rectangular profile with $s_{en} = 5\ s_{opt}$; wavelength unit: FWHM of sinc^2 profile (A)

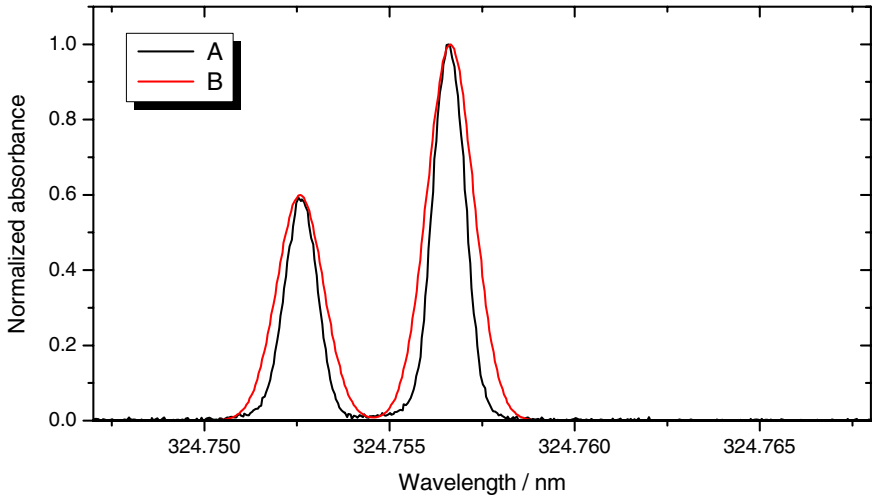

Figure 2.6: Comparison of the line profile of the Cu doublet obtained with a HCL, with a Doppler profile corresponding to 2600 K; A: lamp emission profile for 5 mA HCL current; B: Doppler profile with 1.4 pm FWHM

ELIAS II (LTB Lasertechnik Berlin GmbH, Berlin, Germany), having an instrument profile width of 0.13 pm (FWHM), which is negligible compared to the line width. The measured profiles were used to determine the line positions and intensities of the Cu doublet. For these values Gauss profiles with 1.4 pm FWHM were calculated, representing the Doppler broadening for Cu at 2600 K.

Next, the synthetic Cu profiles were convoluted by a Lorentz profile with 1.1 pm FWMH representing the collisional broadening in a 2600 K flame at normal pressure, and for an assumed collisional cross-section of $2 \cdot 10^{-18}$ m^2 (see Figure 2.2).

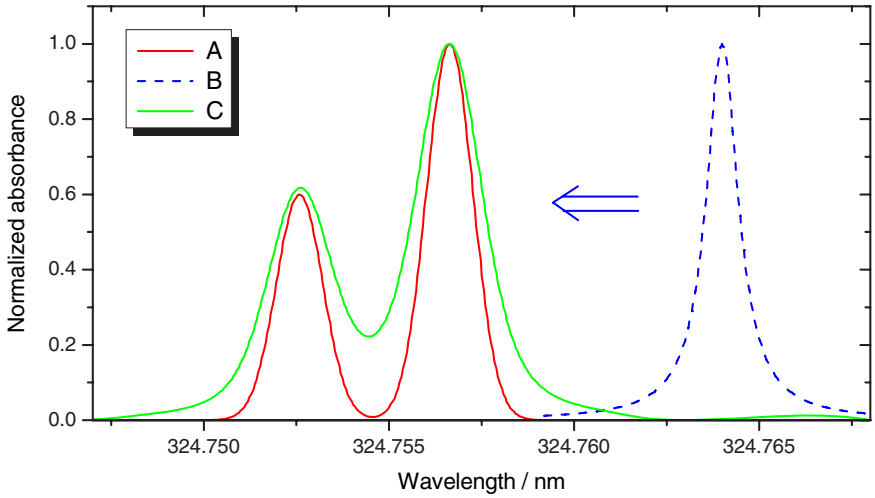

Figure 2.7: Convolution of the synthetic Doppler profile from Figure 2.6 with a Lorentz profile corresponding to 2600 K, normal pressure, and a collisional cross-section of $2 \cdot 10^{-18}$ m^2; A: Doppler profile, B: convoluting Lorentz profile with 1.1 pm FWHM, C: resulting Voigt profile

In a last step, the arising profile was convoluted by a Gauss function with 0.9 pm FWHM, representing the instrument profile of the below-discussed spectrometer SuperDEMON (refer to Chapter 3.2.2) at 324 nm. The calculated profile is faced to an absorbance profile measured in an air / acetylene flame with the SuperDEMON. The comparison shows a satisfying conformity of calculated and measured profiles.

With a numerical deconvolution procedure, corresponding to the convolution method demonstrated above, Voigt widths for some measured analytical lines were determined. The results are collected in Table 2.1 and compared with calculated values corresponding to Equations 2.7, 2.11, and 2.13.

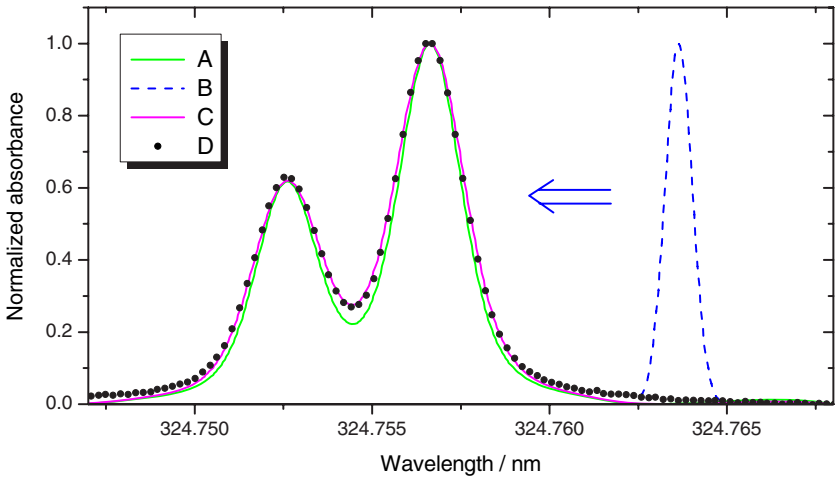

Figure 2.8: Convolution of the synthetic Voigt profile from Figure 2.7 with a Gauss profile representing the instrument function of SuperDEMON; A: Voigt profile; B: convoluting Gauss profile with 0.9 pm FWHM; C: convolution result; D: measured absorbance profile in an air / acetylene flame

Table 2.1: Comparison of measured with calculated FWHM values for Lorentz profiles

Element	Wavelength / nm	Measured $\Delta\lambda_V$ / pm	Calculated $\Delta\lambda_V$ / pm	Ratio measured / calculated
Ag	328.068	1.71	1.77	0.97
Ag	338.289	1.74	1.84	0.94
Ca	422.673	3.39	3.60	0.94
Cd	228.802	1.10	1.07	1.03
Co	240.725	1.73	1.47	1.17
Cr	357.868	2.18	2.60	0.84
Cu	324.754	2.02	2.10	0.96
Cu	327.396	1.99	2.10	0.95
Fe	248.327	1.51	1.56	0.97
Ga	287.424	2.41	1.73	1.40
Ga	294.364	2.19	1.78	1.23
Ga	294.417	2.02	1.79	1.13
Ga	403.299	4.54	2.74	1.66

Table 2.1 (continued)

Element	Wavelength / nm	Measured $\Delta\lambda_V$ / pm	Calculated $\Delta\lambda_V$ / pm	Ratio measured / calculated
Ga	417.204	3.51	2.88	1.22
In	303.936	2.15	1.55	1.39
In	325.609	2.35	1.71	1.38
Ir	208.882	0.79	0.78	1.02
Ir	237.277	1.21	0.92	1.31
Ir	250.298	1.24	1.00	1.24
K	404.414	5.78	3.43	1.69
K	404.721	5.42	3.43	1.58
K	766.491	9.69	8.75	1.11
K	769.897	9.42	8.81	1.07
Li	323.266	6.76	5.54	1.22
Li	670.785	12.04	14.37	0.84
Mg	285.213	2.54	2.68	0.95
Mn	279.482	2.41	1.83	1.31
Mo	313.259	1.48	1.73	0.86
Na	330.237	4.44	3.28	1.35
Na	330.298	4.32	3.29	1.31
Na	588.995	7.42	7.13	1.04
Na	589.592	7.20	7.15	1.01
Pb	217.001	1.19	0.80	1.49
Pb	283.306	1.80	1.16	1.55
Pd	244.791	1.15	1.19	0.96
Pd	247.642	1.19	1.21	0.98
Rh	343.489	1.63	1.91	0.85
Ru	349.895	1.73	1.97	0.88
Sb	217.581	1.47	0.97	1.51
Se	196.026	1.27	1.01	1.25
Se	203.395	1.11	1.06	1.05
Se	206.279	1.22	1.08	1.13
Se	207.480	1.15	1.09	1.06
Sn	224.605	1.15	1.02	1.13
Sn	286.332	1.67	1.41	1.18
Sr	460.733	3.13	3.08	1.02

Table 2.1 (continued)

Element	Wavelength / nm	Measured $\Delta\lambda_V$ / pm	Calculated $\Delta\lambda_V$ / pm	Ratio measured / calculated
Te	214.281	1.09	0.93	1.17
Tl	276.787	1.77	1.12	1.57
Zn	213.856	1.17	1.22	0.96

Another comparison of measured and calculated Voigt profiles is shown in Figure 2.9. The calculated line widths are displayed, as in Figure 2.4, with the molar mass M_A as parameter. The measured values are grouped by the masses of the respective absorbing atoms. The classification is indicated by different colors and is as follows: black $M_A = 7$, green $M_A = 23 \ldots 40$, blue $M_A = 52 \ldots 79$, cyan $M_A = 88 \ldots 128$, and magenta $M_A = 192 \ldots 207$. As can be expected, the significant deviations of the measured from the calculated values are directed to larger line widths, which should be caused by non-resolvable line splitting. For the majority of lines, however, the agreement is satisfactorily and demonstrates the usefulness of the presented approximations.

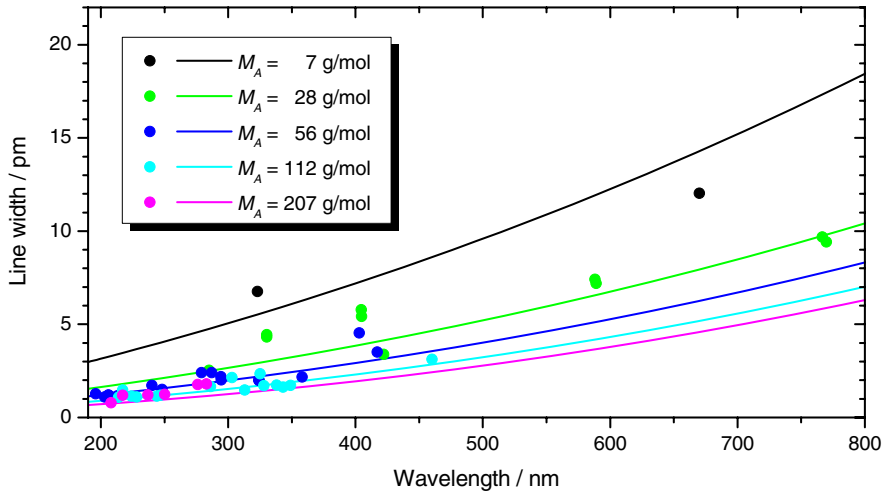

Figure 2.9: Comparison of measured (dots) and calculated (curves) Voigt widths for the absorption lines given in Table 2.1, grouped by atom masses corresponding to values used as parameters for calculated curves